Non-orthogonal spline wavelets for boundary element analysis

Kazuhiro Koro [†], Kazuhisa Abe[*]

Department of Civil Engineering and Architecture, Niigata University
8050 Igarashi 2-Nocho, Niigata, 950-2181, JAPAN

[†]Associate Professor, Fax; +81-25-262-7021, E-mail; kouro@eng.niigata-u.ac.jp
[*]Corresponding author, Associate Professor, Fax; +81-25-262-7021, E-mail; abe@eng.niigata-u.ac.jp

Summary

Non-orthogonal spline wavelets are developed for Galerkin BEM. The proposed wavelets have compact supports and closed-form expressions. Besides of it, one can choose arbitrarily the order of vanishing moments of the wavelets independently of order of B-splines. Sparse coefficient matrices are obtained by truncating the small elements *a priori*. The memory requirement and computational time can be controled by changing the order of vanishing moments of the wavelets. As an iterative technique for solving the boundary element equations, GMRES(m) method is employed. Diagonal scaling and incomplete LU factorization (ILU(0)) are considered for the preconditioning. The ILU(0) becomes an effective preconditioner for higher order vanishing moments. Through numerical examples, availability of the proposed wavelets is investigated.

Key Words

wavelet-BEM; non-orthogonal wavelet; fast solution; 2-D Laplace problem; GMRES

1 Introduction

Boundary element method (BEM) only requires discretization of the boundary. This is the main advantage of the method. However, its computational cost is more expensive than that of finite element method, particularly for large-scale problems. This is because the discretization of the boundary integral equation leads to fully populated coefficient matrices requiring $O(N^2)$ memory storage and $O(N^3)$ computational work (N: degrees of freedom). On the other hand, in the finite element analysis we obtain a sparse stiffness matrix in spite of the large number of unknowns. In recent years, many researchers have attempted to overcome this computational difficulty in BEMs, e.g. by a panel clustering technique[1], a fast multipole method[2] and employment of wavelets. These remedies reduce the computational work to $O(N(\log N)^\alpha)$ or $O(N^{1+\beta})$ where $\alpha \geq 0$ and $0 \leq \beta \leq 1$.

In the application of the wavelet to BEM, two features of the wavelet play an important role in the improvement of the performance, that is, local support and vanishing moments. The vanishing moments imply the orthogonality of the wavelet basis to all polynomials of a certain degree or less. In BEMs, the coefficient matrix is defined as an inner product of the basis and a kernel function. Hence, when the wavelet is used as the basis, due to the vanishing moment property of the wavelets, asymptotical order of the element is increased for large distance between the source and integral points. As a result, most of the matrix entries have small values. This fact enables us to obtain a sparse matrix by truncating the small elements.

The wavelet basis have been applied to integral equations by two ways. One is the employment of the wavelets constructed by linear combination of Dirac delta functions, which have been proposed by Beylkin *et al.*[3], Alpert *et al.*[4] and Canning[5]. In this approach, a discrete wavelet transform is applied to the matrix obtained by the conventional discretization. The same idea has been used to improve the performance of the BEM for collocation method[6][7].

The other approach is the application of continuous wavelet to the basis and the weighting function of BEM. This is referred to as *the wavelet-BEM*. Steinberg *et al.* [8] and Sabetfakhri *et al.* [9] have attempted to employ the Battle-Lemarié wavelet. Wang [10][11] has proposed the boundary element analysis using the Daubechies wavelet. These wavelets are classified in orthonormal wavelet. Although the orthonormal wavelets were employed in many works, they have disadvantages in application to BEM. The Battle-Lemarié wavelet has an infinite support, though its amplitude shows exponential decay. On the other hand, the Daubechies wavelet is not given by a closed-form in spite of a compactly supported wavelet. The authors[7][12] have attempted to use the Haar wavelet. The Haar wavelet is only a compactly supported wavelet with a closed-form. However, the order of its vanishing moments is the lowest one. Therefore this basis does not offer remarkable improvement. In order to avoid those difficulties in the orthonormal wavelets, Goswami *et al.*[13] have employed a semi-orthogonal wavelet, in which bases in the same subspace do not have orthogonality. While for the semi-orthogonal wavelets not all of the bases satisfy the orthogonality, they have compact support and closed-form. Moreover, the

semi-orthogonality permits the integral wavelet transform based on a duality principle[14]. However one cannot control the order of vanishing moments.

In the works mentioned above, the basis functions are orthonormal or semi-orthogonal wavelets. However, the wavelet-BEM owes its effectiveness to the local support and vanishing moment property of the wavelet basis. In this context, the orthogonality of the basis is not a necessary condition.

In the present paper, we develop a non-orthogonal wavelet that is suitable for the boundary element analysis. By using B-splines, this wavelet can be represented in a closed-form. In addition, no any orthogonality is imposed on the bases. This provides a compact support. Furthermore, we can choose the order of vanishing moments independently of the order of B-splines. However, in the application of the present bases we encounter a difficulty, that is, the components of a known vector in algebraic equations have to be evaluated by the fast wavelet transform with matrix inversion. This is because the wavelet transform is not defined as an orthogonal transformation, for the non-orthogonal wavelet. However, this computational work can be reduced to $O(w^2N)$, since the transformation matrix is a band matrix with band width w.

This paper is organized as follows, in Section 2, we describe a multilevel representation for the non-orthogonal wavelets and construction of the non-orthogonal spline wavelet. In wavelet-BEM, since the wavelet expansion is usually defined on a finite interval, a boundary wavelet is required to guarantee the completeness of the bases. Construction of the boundary wavelet is then attempted in Section 3. Moreover, we introduce an algorithm for evaluation of expansion coefficients of a wavelet series. In Section 4, we show boundary element formulation using the wavelets for 2-D Laplace problem, and a truncation strategy of coefficient matrix entries is also shown. In Section 5, we discuss the performance of the method, such as memory requirement and CPU time, based on the numerical results. Finally, concluding remarks are summarized in Section 6.

2 Development of non-orthogonal wavelets

2.1. Multilevel representation using non-orthogonal wavelets

One of the important features of the wavelets is to develop representation of a function at various resolution scale based on the multiresolution analysis (MRA) [15][16].

The MRA in the Hilbert space $L^2(\mathbf{R})$ is given by a sequence of subspaces $\mathbf{V}_k$ with the

following property:

$$\{0\} \subset \cdots \subset \mathbf{V}_{-1} \subset \mathbf{V}_0 \subset \mathbf{V}_1 \subset \cdots \subset L^2(\mathbf{R}), \tag{1}$$

$$\overline{\bigcup_{k\in\mathbf{Z}} \mathbf{V}_k} = L^2(\mathbf{R}), \tag{2}$$

$$\bigcap_{k\in\mathbf{Z}} \mathbf{V}_k = \{0\}, \tag{3}$$

$$\begin{aligned} h(\xi) \in \mathbf{V}_k &\Longleftrightarrow h(2\xi) \in \mathbf{V}_{k+1}, \\ h(\xi) \in \mathbf{V}_k &\Longleftrightarrow \{h(\xi - j),\ j \in \mathbf{Z}\} \in \mathbf{V}_k, \end{aligned} \tag{4}$$

where $\mathbf{R}$ and $\mathbf{Z}$ are sets of all reals and integers, respectively. $h(\xi)$ is an arbitrary function, and the symbol $\overline{\quad}$ represents a closure.

We introduce *a scaling function* ϕ such that

$$\mathbf{V}_k = \mathrm{span}\overline{\{\phi_{k,j}(\xi),\ j \in \mathbf{Z}\}}, \tag{5}$$

$$\phi_{k,j}(\xi) = 2^{\frac{k}{2}}\phi(2^k\xi - j) \qquad (j, k\ \in \mathbf{Z}). \tag{6}$$

Let us consider the two subspaces $\mathbf{V}_k$ and $\mathbf{V}_{k+1}$. From equations (1) and (5), the scaling function ϕ_k that is the basis in $\mathbf{V}_k$ can be expressed as

$$\phi_{k,j}(\xi) = \sum_{l\in\mathbf{Z}} a_l \cdot \phi_{k+1,l}(\xi) \qquad (j \in \mathbf{Z}), \tag{7}$$

where a_l $(l \in \mathbf{Z})$ are coefficients determining a hierarchical relation of the scaling functions. Equation (7) is referred to as *the dilation equation* or *the two-scale relation.*

We define the difference between the subspaces $\mathbf{V}_k$ and $\mathbf{V}_{k+1}$ as a subspace $\mathbf{W}_k$. Hence, the space $\mathbf{V}_{k+1}$ consists of the subspaces $\mathbf{V}_k$ and $\mathbf{W}_k$

$$\mathbf{V}_{k+1} = \mathbf{V}_k + \mathbf{W}_k, \tag{8}$$

where a symbol + denotes direct sum. Note that for the orthonormal or semi-orthogonal wavelet these subspaces are connected by orthogonal sum $\oplus$.

From equations (2) and (8), the direct sum of all complementary subspaces $\mathbf{W}_k$ is dense in $L^2(\mathbf{R})$, that is,

$$L^2(\mathbf{R}) = \overline{\bigcup_{k\in\mathbf{Z}} \mathbf{W}_k}. \tag{9}$$

Now, let us introduce *a wavelet* ψ such that

$$\mathbf{W}_k = \mathrm{span}\overline{\{\psi_{k,j}(\xi),\ j \in \mathbf{Z}\}}, \tag{10}$$

$$\psi_{k,j}(\xi) = 2^{\frac{k}{2}}\psi(2^k\xi - j) \qquad (j, k\ \in \mathbf{Z}). \tag{11}$$

From equation (8), since the space $\mathbf{W}_k$ is the complementary subspace of MRA, the basis $\psi_{k,j}$ in $\mathbf{W}_k$ is constructed by the bases in the space $\mathbf{V}_{k+1}$, i.e.,

$$\psi_{k,j}(\xi) = \sum_{l\in\mathbf{Z}} b_l \cdot \phi_{k+1,l}(\xi), \tag{12}$$

where b_l ($l \in \mathbf{Z}$) are constants.

In cases where the MRA is applied to the interval $[0,1]$, the subspaces $\mathbf{V}_k$ are given as a semi-infinite increasing sequence with initial subspace $\mathbf{V}_0$ instead of an infinite sequence, i.e.,

$$\mathbf{V}_0 \subset \mathbf{V}_1 \subset \cdots \subset \mathbf{V}_k \subset \cdots \subset L^2[0,1]. \tag{13}$$

Then, equation (9) is rewritten as

$$L^2[0,1] = \overline{\mathbf{V}_0 + \bigcup_{k=0}^{\infty} \mathbf{W}_k}. \tag{14}$$

We now consider a projection of an arbitrary function $f(\xi)$ on a subspace. When the projections on the subspaces $\mathbf{V}_0$ and $\mathbf{W}_k$ (k: a positive integer) are defined as $P_0 f$ and $Q_k f$, respectively, from equation (14), $f(\xi)$ can be expressed by superposition of the projections, namely,

$$f(\xi) = P_0 f(\xi) + \sum_{k=0}^{\infty} Q_k f(\xi). \tag{15}$$

In equation (15), the projections $P_0 f$ and $Q_k f$ are given by

$$\begin{aligned} P_0 f(\xi) &= \sum_{j=1}^{N_0} c_{0,j} \phi_{0,j}(\xi), \\ Q_k f(\xi) &= \sum_{l=1}^{n_k} d_{k,l} \psi_{k,l}(\xi), \end{aligned} \tag{16}$$

where $c_{0,j}$ and $d_{k,l}$ are expansion coefficients. N_0 and n_k are the number of bases $\phi_{0,j}$ and $\psi_{k,l}$, respectively.

Substituting equation (16) into (15), we obtain the following representation for the function f:

$$f(\xi) = \sum_{j=1}^{N_0} c_{0,j} \phi_{0,j}(\xi) + \sum_{k=0}^{\infty} \sum_{l=1}^{n_k} d_{k,l} \psi_{k,l}(\xi). \tag{17}$$

Equation (17) is called *the wavelet series.*

2.2. Scaling functions

We use a B-spline as a scaling function [14]. Let ϕ^m denote the scaling function associated with the B-spline of order $(m+1)$:

$$\phi^m(\xi) = \frac{1}{m!} \sum_{j=0}^{m+1} (-1)^j \binom{m+1}{j} (\xi - j)_+^m, \tag{18}$$

where $\binom{m+1}{j}$ is a binomial coefficient. The polynomial $(\xi - j)_+^m$ is termed *the truncated power function*, and is defined by

$$(\xi - j)_+^m = \begin{cases} 0 & (\xi < j), \\ (\xi - j)^m & (\xi \geq j). \end{cases} \tag{19}$$

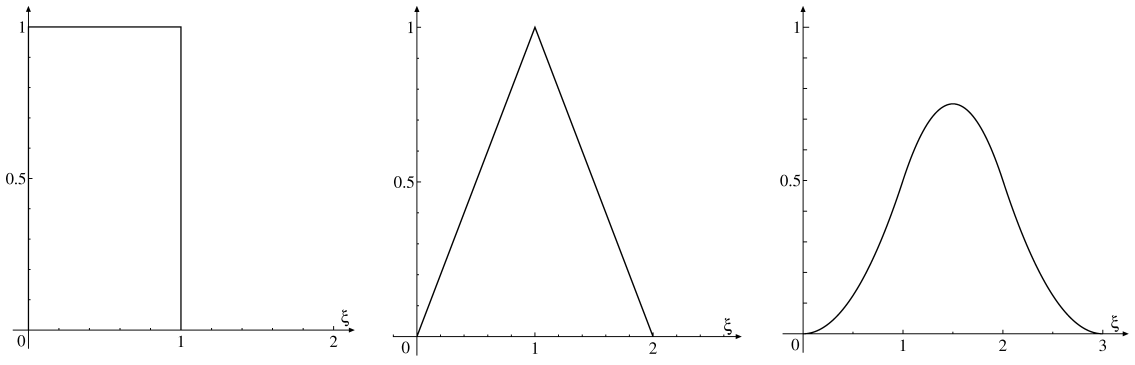

(a) (b) (c)

Figure 1: Examples of the scaling function. (a) Piecewise constant scaling function $\phi^0(\xi)$. (b) Piecewise linear scaling function $\phi^1(\xi)$. (c) Piecewise quadratic scaling function $\phi^2(\xi)$.

Figure 1 depicts the shape of the scaling functions with $m = 0, 1$ and 2.

For the scaling functions given by equation (18), we obtain the dilation equation as follows:

$$\phi^m(\xi) = \frac{1}{2^m} \sum_{j=0}^{m+1} \binom{m+1}{j} \phi^m(2\xi - j). \tag{20}$$

2.3. Wavelets

As shown in the previous subsection, the scaling function is constructed using piecewise polynomials of degree m. When ϕ^m is used as the basis of MRA, the wavelets spanning the complementary subspaces in MRA are required to have a degree of polynomials which equals to that of ϕ^m. Moreover, in this study, the wavelet has the arbitrary-order vanishing moments and compact support.

We now define ψ_n^m as the wavelet that consists of $(m+1)$th-order B-splines and possesses nth-order vanishing moments, i.e.,

$$\int_{-\infty}^{\infty} \xi^k \cdot \psi_n^m(\xi)\, d\xi = 0 \qquad (k = 0, 1, \ldots, n-1). \tag{21}$$

In order to construct the wavelet ψ_n^m, we prepare the following result.

Theorem 2.1. When a function ψ_n^m has nth-order vanishing moments, the function

$$\psi_{n+1}^m(\xi) = \psi_n^m(\xi) - \psi_n^m(\xi - \gamma) \qquad (n \geq 1) \tag{22}$$

has $(n+1)$th-order vanishing moments. In equation (22), $\gamma \neq 0$ is an arbitrary real number.

Proof. It is clear that ψ_{n+1}^m has nth-order vanishing moments. On the other hand, from

equation (22) we have

$$\int_{-\infty}^{\infty} \xi^n \psi_{n+1}^m(\xi)\, d\xi = \int_{-\infty}^{\infty} \xi^n \left[\psi_n^m(\xi) - \psi_n^m(\xi-\gamma)\right]\, d\xi$$
$$= \int_{-\infty}^{\infty} \xi^n \psi_n^m(\xi)\, d\xi - \int_{-\infty}^{\infty} (\xi+\gamma)^n \psi_n^m(\xi)\, d\xi. \tag{23}$$

In the second integration of the right-hand side of equation (23),

$$(\xi+\gamma)^n = \xi^n + \sum_{i=1}^{n} \binom{n}{i} \gamma^{n+1-i} \xi^{i-1}. \tag{24}$$

Substituting equation (24) into (23), we obtain

$$\int_{-\infty}^{\infty} \xi^n \psi_{n+1}^m(\xi)\, d\xi$$
$$= \int_{-\infty}^{\infty} (\xi^n - \xi^n) \psi_n^m(\xi)\, d\xi - \sum_{i=1}^{n} \binom{n}{i} \gamma^{n+1-i} \int_{-\infty}^{\infty} \xi^{i-1} \psi_n^m(\xi)\, d\xi = 0. \tag{25}$$

This completes the proof of *Theorem 2.1.* □

In this study, γ is set to $1/2$ and the wavelet ψ_n^m is given by

$$\psi_1^m(\xi) = \alpha_1^m \left\{\phi^m(2\xi) - \phi(2\xi-1)\right\}, \tag{26}$$

$$\psi_n^m(\xi) = \beta_n^m \left\{\psi_{n-1}^m(\xi) - \psi_{n-1}^m\left(\xi - \frac{1}{2}\right)\right\} \qquad (n \geq 2), \tag{27}$$

where α_1^m and β_n^m are determined as follows:

$$\alpha_1^m = \sqrt{\frac{B^m}{C_1^m}}, \qquad \beta_n^m = \sqrt{\frac{B^m}{C_n^m}}, \tag{28}$$

$$B^m = \int_{-\infty}^{\infty} \{\phi^m(\xi)\}^2\, d\xi, \tag{29}$$

$$C_n^m = \begin{cases} \displaystyle\int_{-\infty}^{\infty} \{\phi^m(2\xi) - \phi^m(2\xi-1)\}^2\, d\xi & (n=1), \\ \displaystyle\int_{-\infty}^{\infty} \left\{\psi_{n-1}^m(\xi) - \psi_{n-1}^m(\xi - \frac{1}{2})\right\}^2 d\xi & (n \geq 2). \end{cases} \tag{30}$$

Throughout this paper, n denotes the order of vanishing moments.

Theorem 2.2. The wavelet can be represented in terms of the truncated power functions by

$$\psi_n^m(\xi) = \frac{\alpha_n^m}{m!} \sum_{j=0}^{m+n+1} (-1)^j \binom{m+n+1}{j} (2\xi - j)_+^m, \tag{31}$$

where α_n^m is a constant calculated by

$$\alpha_n^m = \sqrt{\frac{B^m}{D_n^m}} = \beta_n^m \cdot \alpha_{n-1}^m, \tag{32}$$

$$D_n^m = \frac{1}{(m!)^2} \int_{-\infty}^{\infty} \left\{ \sum_{j=0}^{m+n+1} (-1)^j \binom{m+n+1}{j} (2\xi - j)_+^m \right\}^2 d\xi. \tag{33}$$

Note that B^m can be evaluated by equation (29).

Proof. The proof is accomplished by induction on n. First, assume $n = 1$. From equations (18) and (26), we have

$$\begin{aligned}\psi_1^m(\xi) &= \alpha_1^m \left\{\phi^m(2\xi) - \phi^m(2\xi - 1)\right\} \\ &= \frac{\alpha_1^m}{m!}\left\{(2\xi)_+^m + \sum_{j=1}^{m+1}(-1)^j \binom{m+2}{j}(2\xi - j)_+^m + (-1)^{m+2}(2\xi - m - 2)_+^m\right\} \\ &= \frac{\alpha_1^m}{m!}\sum_{j=0}^{m+2}(-1)^j \binom{m+2}{j}(2\xi - j)_+^m. \end{aligned} \tag{34}$$

Hence, equation (31) holds for $n = 1$.

Next, assume that equation (31) holds for $n = k - 1 \geq 1$. Then it follows from equation (27) and (31) that

$$\begin{aligned}\psi_k^m(\xi) &= \beta_k^m \left\{\psi_{k-1}^m(\xi) - \psi_{k-1}^m\left(\xi - \frac{1}{2}\right)\right\} \\ &= \beta_k^m \cdot \frac{\alpha_{k-1}^m}{m!}\left\{\sum_{j=0}^{m+k}(-1)^j \binom{m+k}{j}(2\xi - j)_+^m - \sum_{j=0}^{m+k}(-1)^j \binom{m+k}{j}(2\xi - j - 1)_+^m\right\} \\ &= \frac{\alpha_k^m}{m!}\sum_{j=0}^{m+k+1}(-1)^j \binom{m+k+1}{j}(2\xi - j)_+^m. \end{aligned} \tag{35}$$

From equation (35), equation (31) holds for $n = k$. Hence, the wavelet ψ_n^m $(n \geq 1)$ can be expressed as equation (31). □

The shape of the wavelets ψ_n^0, ψ_n^1 and ψ_n^2 (for $n = 1, 2, 3$) are shown in Figure 2, Figure 3 and Figure 4, respectively. Moreover, examples of the values of α_n^m are summarized in Table 1.

Theorem 2.3. For the proposed non-orthogonal wavelets, the two-scale relation between the wavelet and the scaling functions is given by

$$\psi_n^m(\xi) = \alpha_n^m \sum_{j=0}^{n}(-1)^j \binom{n}{j}\phi^m(2\xi - j). \tag{36}$$

Proof. Equation (36) is proved by induction on n.

First, assume $n = 1$. From equation (18), we have

$$\begin{aligned}\psi_1^m(\xi) &= \alpha_1^m \left\{\phi^m(2\xi) - \phi^m(2\xi - 1)\right\} \\ &= \alpha_1^m \sum_{j=0}^{1}(-1)^j \binom{1}{j}\phi^m(2\xi - j). \end{aligned} \tag{37}$$

Hence, equation (36) holds for $n = 1$.

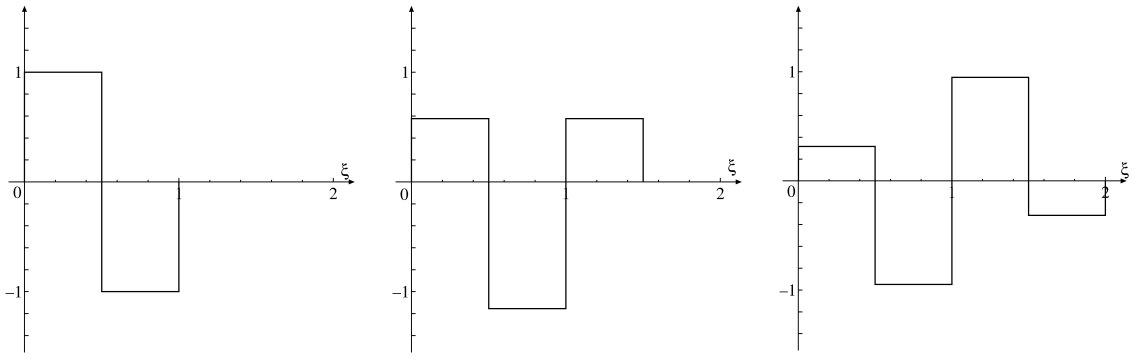

(a) (b) (c)

Figure 2: Piecewise constant non-orthogonal wavelets. (a) Wavelet $\psi_1^0(\xi)$. (b) Wavelet $\psi_2^0(\xi)$. (c) Wavelet $\psi_3^0(\xi)$.

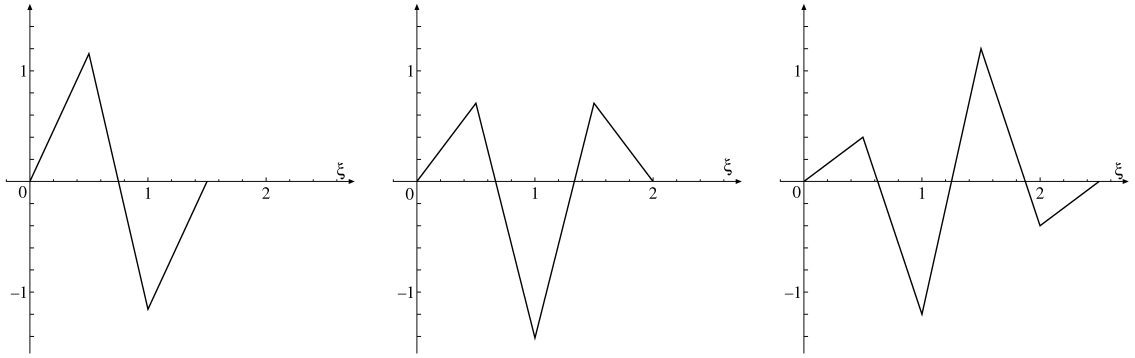

(a) (b) (c)

Figure 3: Piecewise linear non-orthogonal wavelets. (a) Wavelet $\psi_1^1(\xi)$. (b) Wavelet $\psi_2^1(\xi)$. (c) Wavelet $\psi_3^1(\xi)$.

Next, we assume that ψ_n^m satisfies equation (36) for $n = k - 1 \geq 1$. It follows from equations (27), (31) and (36) that

$$\begin{aligned}
\psi_k^m(\xi) &= \beta_k^m \left\{ \psi_{k-1}^m(\xi) - \psi_{k-1}^m\left(\xi - \frac{1}{2}\right) \right\} \\
&= \alpha_{k-1}^m \beta_k^m \left\{ \sum_{j=0}^{k-1} (-1)^j \binom{k-1}{j} \phi^m(2\xi - j) - \sum_{j=0}^{k-1} (-1)^j \binom{k-1}{j} \phi^m(2\xi - j - 1) \right\} \\
&= \alpha_k^m \sum_{j=0}^{k} (-1)^j \binom{k}{j} \phi^m(2\xi - j). \qquad (38)
\end{aligned}$$

Hence, equation (36) holds for $n \geq 1$. □

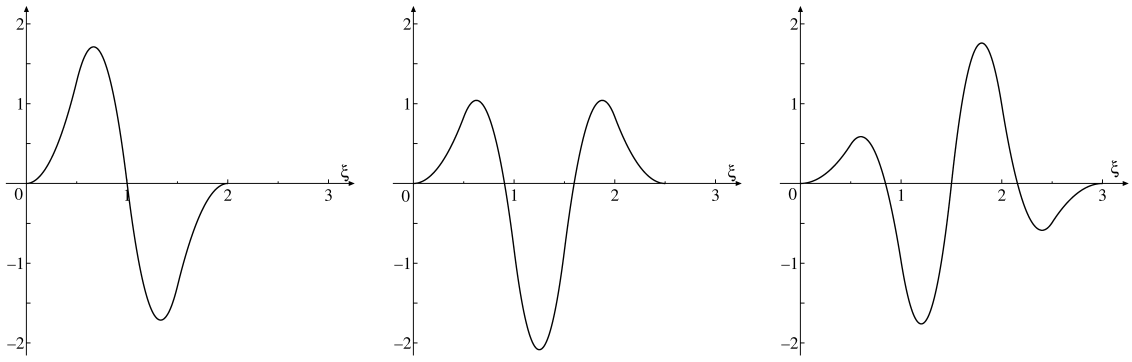

(a) (b) (c)

Figure 4: Piecewise quadratic non-orthogonal wavelets. (a) Wavelet $\psi_1^2(\xi)$. (b) Wavelet $\psi_2^2(\xi)$. (c) Wavelet $\psi_3^2(\xi)$.

Table 1: Examples of values of α_n^m (m: degree of polynomials, n: order of vanishing moments).

m	n	α_n^m
0	1	1
	2	$1/\sqrt{3}$
	3	$1/\sqrt{10}$
	4	$1/\sqrt{35}$
1	1	$2/\sqrt{3}$
	2	$1/\sqrt{2}$
	3	$2/5$
2	1	$\sqrt{33/20}$
	2	$\sqrt{66/95}$
	3	$\sqrt{11/46}$

3 Wavelet expansion on a finite interval

The proposed non-orthogonal wavelets form the bases in the space $L^2(\mathbf{R})$. Using these bases, an arbitrary function in $L^2(\mathbf{R})$ can be expressed as the wavelet series. On the other hand, for an interval, one cannot complete the wavelet series by using only these bases. This is because supports of some bases are truncated at the left or right endpoint of the interval. Hence, special bases have to be introduced into the wavelet expansion on the finite interval. These functions are distinguished from the bases given by equations (18) and (31), and are referred to as *the boundary scaling function* and *the boundary wavelet*.

The wavelet expansion has to keep symmetry of an expanded function on a finite interval.

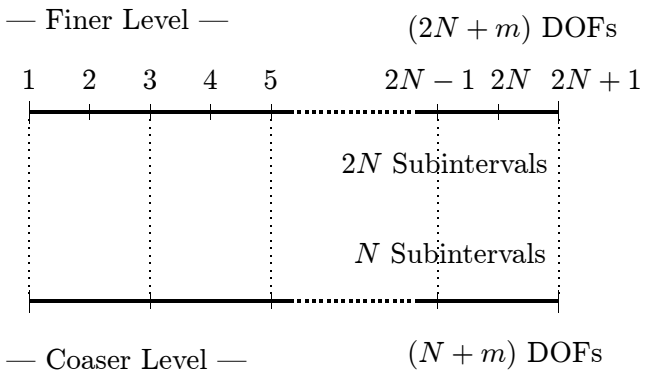

Figure 5: Finite interval under two-scale subdivision. The number of subintervals and DOFs are N and $(N+m)$ for coaser scale, $2N$ and $(2N+m)$ for finer scale, respectively. In finer scale, $(2N+1)$ knots are required.

This requires to arrange the bases so that the location of them can be symmetry with respect to center of the interval. In order to accomplish this arrangement, the degree m of polynomials and the order n of vanishing moments are determined such that a sum $(m+n)$ is odd.

3.1. Boundary scaling functions

In this study, a scaling function is given as a B-spline. When we employ $\phi^m(\xi)$ for the scaling function, m kinds of scaling function are required as the bases at each endpoint of the interval. These scaling functions are defined as B-splines with multiple knots.

3.2. Boundary wavelets

a. Number of boundary wavelets

To discuss the number of boundary wavelets, let us consider an interval which is divided by two resolution levels into N and $2N$ subintervals, as shown in Figure 5.

Assume that ϕ^m and ψ_n^m are used as the bases. Then, the DOFs in each scale are $(N+m)$ and $(2N+m)$, respectively. Since the difference of the DOFs in both scales has to be equal to the number of added wavelets, N wavelets are necessary to obtain the finer resolution approximation.

In the finer scale, there are $(2N+1)$ knots for $2N$ subdivisions. When these knots are numbered from the left endpoint in order as shown in Figure 5, the added wavelets are arranged so that the center of their support may coinside with one of the even knots. This is because the wavelets always have even $(m+n+1)$ subintervals. Hence, in order to avoid the truncation of the wavelet support, the wavelet that is the closest to the endpoint of

Table 2: Number of boundary wavelets N_b.

		m			
		0	1	2	3
n	1	0	—	1	—
	2	—	1	—	1
	3	1	—	1	—
	4	—	1	—	2
	5	1	—	2	—
	6	—	2	—	2

the interval has to satisfy the following inequality:

$$2j > \frac{m+n+1}{2}, \tag{39}$$

where $2j$ denotes a knot number corresponding to the center of the support.

Then, the number of boundary wavelets N_b is determined by

$$N_b = j' - 1, \tag{40}$$

where j' is a minimum integer of j 's satisfying the above inequality (39).

Consequently, in a certain scale, N wavelets consist of $2N_b = 2(j'-1)$ boundary wavelets and $(N - 2N_b)$ wavelets. Examples of the values of N_b are summarized in Table 2.

b. Development of piecewise constant boundary wavelets

In cases where a scaling function and a wavelet are constructed by piecewise polynomials of degree $m = 0$, i.e., piecewise constant functions, no boundary scaling functions are required for construction of the bases. On the other hand, the number of boundary wavelets is determined based on the order of vanishing moments n. In this study, we employ the wavelets with higher order vanishing moments than n as the required boundary wavelets $\bar{\psi}^0_{in}$, that is,

$$\bar{\psi}^0_{in}(\xi) = \psi^0_{n+i}(\xi) \qquad (i = 1, 2, \ldots, N_b). \tag{41}$$

c. Development of boundary wavelets with $m \geq 1$

When the bases are constructed by a scaling function ϕ^m and a wavelet ψ^m_n $(m \geq 1)$, the boundary scaling functions $\bar{\phi}^m_i$ $(i = 1, 2, \ldots, m)$ are required, besides N_b boundary wavelets. In this paper, we construct the boundary wavelets for $N_b \leq m$. When $N_b \leq m$, the N_b boundary wavelets $\bar{\psi}^m_{i1}$ $(i = 1, 2, \ldots, N_b)$ having first-order vanishing moments can be constructed by linear combination of ϕ^m and $\bar{\phi}^m_i$, namely,

$$\bar{\psi}^m_{i1}(\xi) = \begin{cases} \bar{\alpha}^m_{i1}\left[\bar{\phi}^m_1(2\xi) + p_i \cdot \bar{\phi}^m_{i+1}(2\xi)\right] & (i < m), \\ \bar{\alpha}^m_{m1}\left[\bar{\phi}^m_1(2\xi) + p_m \cdot \phi^m(2\xi)\right] & (i = m), \end{cases} \tag{42}$$

where p_i and p_m are determined so that the wavelet $\bar{\psi}_{i1}^m$ may have the first order vanishing moment.

Once the wavelets $\bar{\psi}_{i1}^m$ are obtained, the N_b boundary wavelets which have nth-order vanishing moments can be defined recursively, for $n \geq 2$, as

$$\bar{\psi}_{in}^m(\xi) = \bar{\alpha}_{in}^m \left[\bar{\psi}_{i(n-1)}^m(\xi) + a_{i,n-1} \cdot \psi_{n-1}^m(\xi) \right] = \bar{\alpha}_{in}^m \left\{ \bar{\psi}_{i1}^m + \sum_{j=1}^{n-1} a_{i,j} \psi_j^m(\xi) \right\} \qquad (n \geq 2,\ i = 1, 2, \ldots, N_b), \tag{43}$$

$\bar{\alpha}_{in}^m$ $(i = 1, 2, \ldots, N_b)$ are constants for the normalization:

$$\int_{-\infty}^{\infty} \{\phi^m(\xi)\}^2 \, d\xi = \int_0^{\infty} \left\{\bar{\psi}_{in}^m(\xi)\right\}^2 \, d\xi \qquad (i = 1, 2, \ldots, N_b). \tag{44}$$

Moreover, the values of $a_{i,n-1}$ are determined so that the wavelet ψ_{in}^m can satisfy the nth-order vanishing moments,

$$a_{i,n-1} = -\frac{\displaystyle\int_0^{\infty} \xi^{n-1} \bar{\psi}_{i1}^m(\xi) \, d\xi + \sum_{j=1}^{n-2} a_{i,j} \int_0^{\infty} \xi^{n-1} \psi_j^m(\xi) \, d\xi}{\displaystyle\int_0^{\infty} \xi^{n-1} \psi_{n-1}^m(\xi) \, d\xi} \qquad (i = 1, 2, \ldots, N_b). \tag{45}$$

The number of boundary wavelets increases as the order of vanishing moments increased. The development of the boundary wavelets for more general case ($N_b > m$) remains to be done at the present time.

Theorem 3.1. From equations (36) and (43), $\bar{\psi}_{in}^m$ $(i = 1, 2, \ldots, N_b, n \geq 2)$ have the two-scale relation described in terms of ϕ^m and $\bar{\psi}_{i1}^m$, which contains ϕ^m and $\bar{\phi}_i^m$, as follows:

$$\bar{\psi}_{in}^m(\xi) = \bar{\alpha}_{in}^m \left[\bar{\psi}_{i1}^m(\xi) + \frac{1}{m!} \sum_{k=0}^{n-1} (-1)^k \phi^m(2\xi - k) \sum_{j=k}^{n-1} a_{i,j} \alpha_j^m \binom{j}{k} \right]. \tag{46}$$

Note that α_0^m and $a_{i,0}$ are equal to zero.

Proof. The proof of equation (46) is accomplished by induction on n. If we assume $n = 2$, then from equations (36) and (43), we have

$$\begin{aligned} \bar{\psi}_{i2}^m(\xi) &= \bar{\alpha}_{i2}^m \left[\bar{\psi}_{i1}^m(\xi) + a_{i,1} \frac{\alpha_1^m}{m!} \sum_{j=0}^{1} (-1)^j \binom{1}{j} \phi^m(2\xi - j) \right] \\ &= \bar{\alpha}_{i2}^m \left[\bar{\psi}_{i1}^m(\xi) + \frac{1}{m!} \sum_{k=0}^{1} (-1)^k \phi^m(2\xi - k) \sum_{j=k}^{1} a_{i,j} \alpha_j^m \binom{j}{k} \right]. \end{aligned} \tag{47}$$

Let us assume that equation (46) holds for $n = k - 1 \geq 2$. Then, $\bar{\psi}_{ik}^m$ is given as

$$\begin{aligned}\bar{\psi}_{ik}^m(\xi) = \bar{\alpha}_{ik}^m \Bigg\{ \bar{\psi}_{i1}^m(\xi) + \frac{1}{m!} \Bigg[\sum_{l=0}^{k-2} (-1)^l \phi^m(2\xi - l) \sum_{j=l}^{k-1} a_{i,j} \alpha_j^m \binom{j}{l} \\ + a_{i,k-1} \cdot \alpha_{k-1}^m (-1)^{k-1} \binom{k-1}{k-1} \phi^m(2\xi - k + 1) \Bigg] \Bigg\} \\ = \bar{\alpha}_{ik}^m \left[\bar{\psi}_{i1}^m(\xi) + \frac{1}{m!} \sum_{l=0}^{k-1} (-1)^l \phi^m(2\xi - l) \sum_{j=l}^{k-1} a_{i,j} \alpha_j^m \binom{j}{l} \right]. \end{aligned} \tag{48}$$

From equations (47) and (48), equation (46) holds for $n \geq 2$. □

Examples of piecewise linear and quadratic boundary wavelets are shown in Figure 6 and Figure 7.

3.3. Evaluation of expansion coefficients

When we attempt to obtain the wavelet series of a function as equation (17), evaluation of expansion coefficients $c_{0,j}$ and $d_{k,j}$ is required. In general, these values are computed using a fast wavelet transform (FWT). For orthonormal bases, this computational work is $O(N^2)$ because of the orthogonality; besides, that can decrease in $O(N)$ if these bases have local supports. For semi-orthogonal bases, the expansion coefficients can also be rapidly computed using the dual bases and algorithm as shown in [16].

In this subsection, we develop a fast algorithm for the evaluation of $c_{0,j}$ and $d_{k,j}$ in non-orthogonal wavelets. In this algorithm, $c_{0,j}$ and $d_{k,j}$ are evaluated based on FWT as illustrated in Figure 8, like conventional methods. The transformation at every scale is accomplished by solving linear algebraic equations derived from the two-scale relation of the bases.

Now, let us seek two-scale relation of the bases spanned subspaces $\mathbf{V}_k$, $\mathbf{V}_{k+1}$ and $\mathbf{W}_k$. When projections of $f \in L^2[0,1]$ on the subspaces $\mathbf{V}_k$, $\mathbf{V}_{k+1}$ and $\mathbf{W}_k$ are defined as $P_k f$, $P_{k+1} f$ and $Q_k f$, from equation (8) the following basis representation is obtained:

$$\sum_{j=1}^{N_{k+1}} c_{k+1,j} \phi_{k+1,j}(\xi) = \sum_{j=1}^{N_k} c_{k,j} \phi_{k,j}(\xi) + \sum_{l=1}^{n_k} d_{k,l} \psi_{k,l}(\xi), \tag{49}$$

where N_k, N_{k+1} and n_k are the number of the bases in the subspaces $\mathbf{V}_k$, $\mathbf{V}_{k+1}$ and $\mathbf{W}_k$, respectively.

Equation (49) is rewritten by

$$\mathbf{C}_{k+1}^T \mathbf{N}_{k+1} = \hat{\mathbf{C}}_k^T \hat{\mathbf{N}}_k, \tag{50}$$

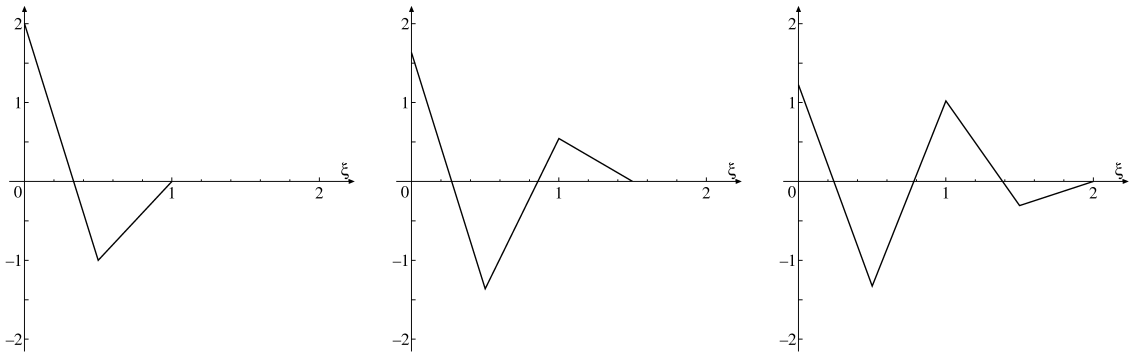

(a) (b) (c)

Figure 6: Piecewise linear boundary wavelets. (a) Boundary wavelet $\bar{\psi}_{11}^1$. (b) Boundary wavelet $\bar{\psi}_{12}^1$. (c) Boundary wavelet $\bar{\psi}_{13}^1$.

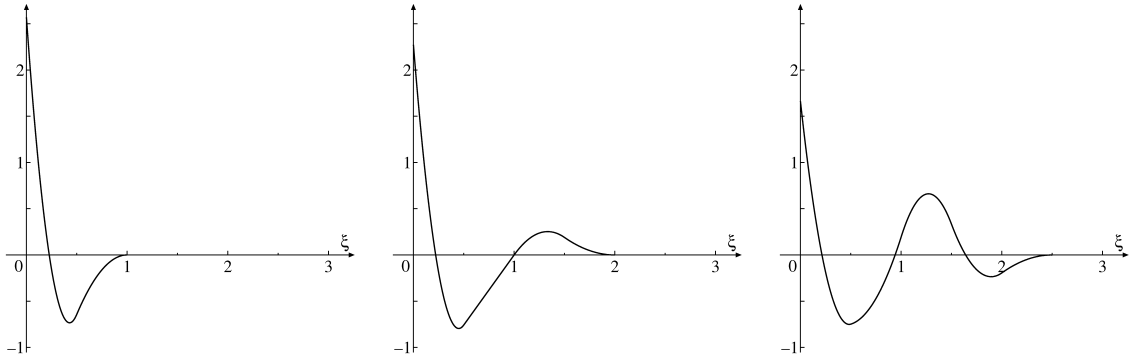

(a) (b) (c)

Figure 7: Piecewise quadratic boundary wavelets. (a) Boundary wavelet $\bar{\psi}_{11}^2$. (b) Boundary wavelet $\bar{\psi}_{12}^2$. (c) Boundary wavelet $\bar{\psi}_{13}^2$.

where

$$\begin{aligned} \hat{\mathbf{C}}_k &= \{c_{k,1}, d_{k,1}, \ldots, c_{k,N_k-1}, d_{k,n_k}, c_{k,N_k}\}^T, \\ \mathbf{C}_{k+1} &= \{c_{k+1,1}, c_{k+1,2}, \ldots, c_{k+1,N_{k+1}}\}^T, \end{aligned} \tag{51}$$

$$\begin{aligned} \hat{\mathbf{N}}_k &= \{\phi_{k,1}, \psi_{k,1}, \ldots, \phi_{k,N_k-1}, \psi_{k,n_k}, \phi_{k,N_k}\}^T, \\ \mathbf{N}_{k+1} &= \{\phi_{k+1,1}, \phi_{k+1,2}, \ldots, \phi_{k+1,N_{k+1}}\}^T. \end{aligned} \tag{52}$$

Moreover, the two-scale relations of the bases can be expressed by

$$\hat{\mathbf{N}}_k = \mathbf{B}_k \mathbf{N}_{k+1}, \tag{53}$$

where $\mathbf{B}_k$ is the transformation matrix whose elements are given by equations (20), (31) and (46).

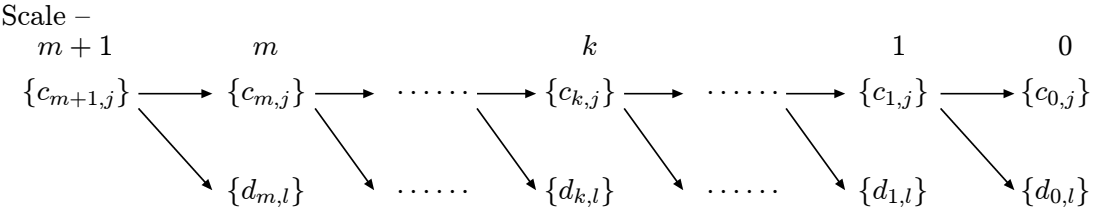

Figure 8: Fast wavelet transform. Expansion coefficients are evaluated in order as shown the arrows in this figure.

Substituting equation (53) into (50), the two-scale relation of the expansion coefficients are described as follows:

$$\mathbf{B}_k^T \hat{\mathbf{C}}_k = \mathbf{C}_{k+1}. \tag{54}$$

In the present method, the expansion coefficients are computed by solving equation (54) with respect to $\hat{\mathbf{C}}_k$, which requires matrix inversion. However its computational cost can be reduced to $O(w^2 N)$, since the transformation matrix $\mathbf{B}_k$ is a band matrix with band width w.

4 Formulation for boundary element analysis

4.1. Boundary element formulations for 2-D Laplace problems

In 2-D Laplace problem, a boundary integral equation is represented by

$$c(\mathbf{x})u(\mathbf{x}) + \int_\Gamma q^*(\mathbf{x},\mathbf{y})u(\mathbf{y})\, d\Gamma_y = \int_\Gamma u^*(\mathbf{x},\mathbf{y})q(\mathbf{y})\, d\Gamma_y \qquad (\mathbf{x},\ \mathbf{y} \in \Gamma), \tag{55}$$

where u and q are the potential and the flux, respectively. u^* and q^* are the fundamental solutions corresponding to u and q. c is the free term, and Γ is the boundary.

To discretize equation (55), we now introduce the wavelet series into the approximation of the solutions u and q, that is,

$$\begin{aligned} \tilde{u}(\xi) &= \sum_{j=1}^{n_b \cdot n_s} \hat{u}_{0,j}\phi_{0,j}(\xi) + \sum_{k=0}^{m_r}\sum_{l=1}^{n_b \cdot n_k} \tilde{u}_{k,l}\psi_{k,l}(\xi), \\ \tilde{q}(\xi) &= \sum_{j=1}^{n_b \cdot n_s} \hat{q}_{0,j}\phi_{0,j}(\xi) + \sum_{k=0}^{m_r}\sum_{l=1}^{n_b \cdot n_k} \tilde{q}_{k,l}\psi_{k,l}(\xi), \end{aligned} \tag{56}$$

where $\hat{u}_{0,j}$, $\hat{q}_{0,j}$, $\tilde{u}_{k,l}$ and $\tilde{q}_{k,l}$ are the expansion coefficients, and m_r is the finest scale. n_s and n_k ($k \geq 0$) are the number of bases $\phi_{0,j}$ and $\psi_{k,l}$, respectively. n_b is the number of finite intervals on boundary.

Substituting equation (56) into equation (55), we obtain a residual $r \neq 0$ defined by

$$r(\mathbf{x}) := c(\mathbf{x})\tilde{u}(\mathbf{x}) + \int_\Gamma q^*(\mathbf{x},\mathbf{y})\tilde{u}(\mathbf{y})\, d\Gamma_y - \int_\Gamma u^*(\mathbf{x},\mathbf{y})\tilde{q}(\mathbf{y})\, d\Gamma_y. \tag{57}$$

The boundary element equation is derived based on the Galerkin method, i.e.,

$$\int_\Gamma r \cdot w_i\, d\Gamma = 0 \qquad (i = 1, 2, \ldots, N), \tag{58}$$

where w_i $(i = 1, 2, \ldots, N)$ are the weighting functions and consist of the bases $\phi_{0,j}$ and $\psi_{k,l}$ as

$$\{w_i |\ i = 1, 2, \ldots, N\} = \left\{\phi_{0,j},\ \psi_{k,l} |\ j = 1, 2, \ldots, n_s,\ k = 0, 1, \ldots, m_r,\ l = 1, 2, \ldots, n_k\right\}. \tag{59}$$

Finally, we obtain the following linear algebraic equations like conventional BEMs:

$$\mathbf{A}\mathbf{z} = \mathbf{b}, \tag{60}$$

where $\mathbf{z}$ is the unknown vector, and $\mathbf{b}$ is the known vector calculated by using the known expansion coefficients evaluated by the above algorithm. $\mathbf{A}$ is a matrix whose elements are given by either g_{ij} or h_{ij}. Here, the matrix elements g_{ij} and h_{ij} are calculated by

$$\begin{aligned} g_{ij} &= \int_{\Gamma_i} w_i \int_{\Gamma_j} u^* w_j \, d\Gamma^2, \\ h_{ij} &= \frac{1}{2}\int_{\Gamma_i} w_i w_j \, d\Gamma + \int_{\Gamma_i} w_i \int_{\Gamma_j} q^* w_j \, d\Gamma^2 \qquad\qquad (i, j = 1, 2, \ldots, N). \end{aligned} \tag{61}$$

4.2. Truncation of matrix entries

In wavelet BEM, most of coefficients g_{ij} and h_{ij} have small values because of the vanishing moment property of the bases. This allows us to generate the *sparse* coefficient matrix $\mathbf{A}$ by truncation of its small entries. Particularly, when we derive the boundary element equations by the Galerkin method, we obtain more sparse matrices than that for the collocation method. However, the discretization by the Galerkin method causes increase in the computational work, since the matrix entries are calculated through double integrations. For the present scaling function and wavelet, its cost increases remarkably. This is because these bases are constructed by a number of piecewise polynomials. In order to reduce the work, we generate a sparse matrix by omitting the computation of the small entries. To do so, selection of the small elements is carried out *a priori* based on estimation of those values.

The absolute values of g_{ij} and h_{ij} of equation (61) can be approximated asymptotically as

$$\begin{aligned} |g_{ij}| \simeq \bar{g}_{ij} &= \frac{\bar{\ell}_i^{n\beta_i+1}\ \bar{\ell}_j^{n\beta_j+1}\ \{n(\beta_i+\beta_j)-1\}!}{(m+1)^{2-\beta_i-\beta_j}} \cdot \left\{\frac{\alpha_n^m}{(m+n+1)^{n+1}}\right\}^{\beta_i+\beta_j} \cdot \frac{2^{-\frac{2n+1}{2}(k_i+k_j)}}{r_0^{n(\beta_i+\beta_j)}}, \\ |h_{ij}| \simeq \bar{h}_{ij} &= \frac{\bar{\ell}_i^{n\beta_i+1}\ \bar{\ell}_j^{n\beta_j+1}\ \{n(\beta_i+\beta_j)\}!}{(m+1)^{2-\beta_i-\beta_j}} \cdot \left\{\frac{\alpha_n^m}{(m+n+1)^{n+1}}\right\}^{\beta_i+\beta_j} \cdot \frac{2^{-\frac{2n+1}{2}(k_i+k_j)}}{r_0^{n(\beta_i+\beta_j)+1}}, \end{aligned} \tag{62}$$

where r_0 is the distance between supports of w_i and w_j, and $\bar{\ell}$ is the length of the support of ϕ_0. k is the resolution scale, and $k = 0$ for $w(\xi) = \phi(\xi)$. Moreover, β is the parameter whose value is equal to 0 for $w(\xi) = \phi(\xi)$ or 1 for $w(\xi) = \psi(\xi)$.

From equation (62), if $r_0 \gg 1$, then $\bar{g}_{ij}$ is greater than $\bar{h}_{ij}$. This is because $\bar{h}_{ij}$ has higher asymptotical order of $1/r_0$ than that of $\bar{g}_{ij}$. Hence, when $\bar{g}_{ij}$ satisfies the following

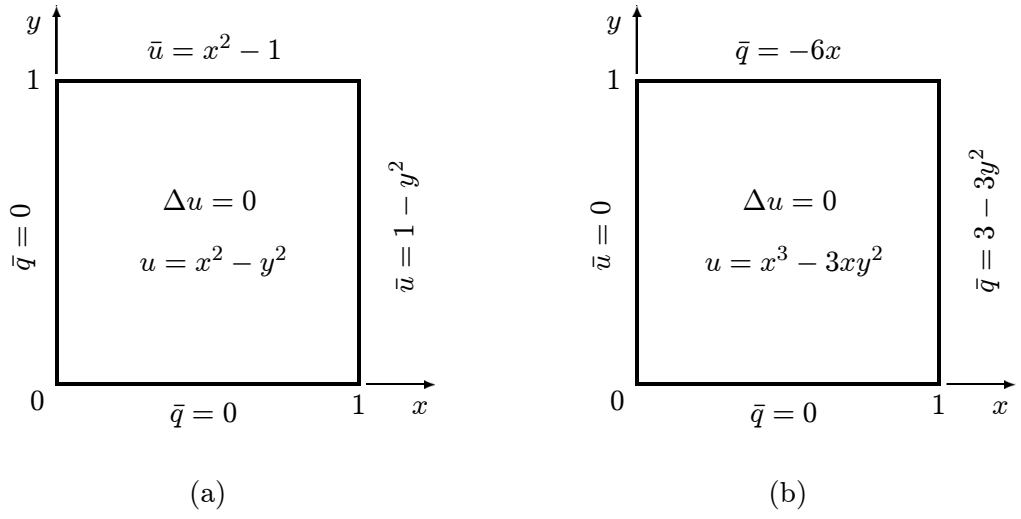

Figure 9: Boundary conditions and exact solution in examples. (a) Ex.1. (b) Ex.2.

inequality, the coefficients g_{ij} and h_{ij} are not computed:

$$\bar{g}_{ij} < \eta \cdot g_{max}, \tag{63}$$

where g_{max} is the maximum value of $|g_{ij}|$ evaluated for $w_i = \phi_i$ and $w_j = \phi_j$. η is a threshold parameter.

When $\bar{g}_{ij}$ does not satisfy inequality (63), the matrix elements are calculated by equation (61). Furthermore, if the elements satisfy the following conditions, they are truncated after the calculation;

$$|g_{ij}| < \eta \cdot g_{max}, \qquad |h_{ij}| < \eta \cdot h_{max}, \tag{64}$$

where h_{max} is the maximum value of $|h_{ij}|$ defined like g_{max}.

5 Numerical results

In this section, we investigate the computational performance of the boundary element analysis and discuss the efficiency of the proposed non-orthogonal wavelets through numerical results.

5.1. Analytical conditions

The present method was applied to 2-D Laplace problems with boundary conditions and exact solution as shown in Figure 9. In both examples, the boundary was divided into four finite intervals, and the piecewise constant and the piecewise linear non-orthogonal wavelets were employed for the bases. The order of vanishing moments of them was set to $n = 1$ or 3 for piecewise constant wavelets, and $n = 2$ or 4 for piecewise linear wavelets. The boundary element equations were solved using the preconditioned GMRES(10) [17], and diagonal scaling or incomplete LU factorization (ILU(0)) was used for the preconditioning. The iteration was stopped when the convergence condition $||\mathbf{r}||/||\mathbf{b}|| < 1.0 \times 10^{-10}$ ($\mathbf{r}$:

residual vector of the iterative solution) was satisfied.

In this experiments, the computational performance of the wavelet-BEM is investigated under the optimal threshold parameter. The optimal threshold parameter is selected from 10 values of $\eta = 1.0 \times 10^{-\delta}$ (δ: integer from 2 to 11), such that, in a certain DOF, the memory requirement becomes the smallest without deterioration of the accuracy. The accuracy of the boundary element solution is estimated by L^2 norm of the error corresponding to the potential on boundary. In general, the optimal threshold parameter should be determined *a priori* so that the truncation error will be comparable to the discretization error [18]. Although determination of the optimal value is necessary in a practical use of the wavelet-BEM, this is out of scope this paper. This issue will be discussed in [19] by the authors.

5.2. Piecewise constant wavelets

In the case of the piecewise constant wavelets, the wavelet expansion is defined on $L^2[0, a]$ where $a = 1$ for $n = 1$ and $a = 3$ for $n = 3$. Note that the interval $[0, a]$ is defined on an intrinsic coodinate corresponding to each subboundary.

The scaling functions $\{\phi_{k,j},\ j = 1, 2, \dots N_k\}$ and those dilation equations are expressed as

$$\phi_{k,j}(\xi) = 2^{\frac{k}{2}} \qquad (j - 1 \le \xi \le j), \tag{65}$$

$$\phi_{k,j} = \frac{1}{\sqrt{2}} \{\phi_{k+1,2j-1} + \phi_{k+1,2j}\} \qquad (j = 1, 2, \dots, N_k), \tag{66}$$

where $N_k = 2^k \cdot a$.

The wavelets $\{\psi_{k,l},\ l = 1, 2, \dots, n_k\}$ where $n_k = 2^k \cdot a$ are given by

$$\psi_{k,l}(\xi) = \frac{1}{\sqrt{2}} \sum_{i=0}^{1} (-1)^i \phi_{k+1,2l+i-1}(\xi) \qquad (l = 1, 2, \dots, n_k), \tag{67}$$

for $n = 1$, and

$$\begin{aligned}
\psi_{k,1}(\xi) &= \frac{1}{\sqrt{35}} \sum_{i=0}^{4} (-1)^i \binom{4}{i} \phi_{k+1,i+1}(\xi), \\
\psi_{k,l}(\xi) &= \frac{1}{\sqrt{10}} \sum_{i=0}^{3} (-1)^i \binom{3}{i} \phi_{k+1,2l+i}(\xi) \qquad (l = 2, 3, \dots n_k - 1), \\
\psi_{k,n_k}(\xi) &= \frac{1}{\sqrt{35}} \sum_{i=0}^{4} (-1)^i \binom{4}{i} \phi_{k+1,N_{k+1}-i}(\xi) = \psi_{k,1}(a - \xi),
\end{aligned} \tag{68}$$

for $n = 3$. Note that the wavelet with $n = 1$ is *the Haar wavelet.*

5.3. Piecewise linear wavelets

For the piecewise linear scaling functions and wavelets, we consider the wavelet expansion on finite intervals $[0, 2]$ for $n = 2$ and $[0, 3]$ for $n = 4$.

The scaling functions are expressed as follows:

$$\begin{aligned}
&\phi_{k,1}(\xi) = 2^{\frac{k+1}{2}}(1-2^k\xi) && (0 \le \xi \le 2^{-k}),\\
&\phi_{k,j}(\xi) = \sum_{i=0}^{2}(-1)^i \binom{2}{i}(2^k\xi - i - j + 2)_+ && (j = 2,3,\ldots,N_k-1),\\
&\phi_{k,N_k}(\xi) = \phi_{k,1}(a-\xi) && (a = 2\,(n=2)\ \text{or}\ 3\,(n=3)),
\end{aligned} \tag{69}$$

where N_k is equal to $2^{k+1}+1$ for $n=2$, and $3\cdot 2^k+1$ for $n=4$. Then, the dilation equations are expressed as

$$\begin{aligned}
&\phi_{k,1} = \frac{1}{\sqrt{2}}\phi_{k+1,1} + \frac{1}{2}\phi_{k+1,2},\\
&\phi_{k,j} = \frac{1}{2\sqrt{2}}\phi_{k+1,2j-2} + \frac{1}{\sqrt{2}}\phi_{k+1,2j-1} + \frac{1}{2\sqrt{2}}\phi_{k+1,2j} && (j = 2,3,\ldots N_k-1),\\
&\phi_{k,N_k} = \frac{1}{2}\phi_{k+1,N_{k+1}-1} + \frac{1}{\sqrt{2}}\phi_{k+1,N_{k+1}}.
\end{aligned} \tag{70}$$

On the other hand, the wavelets are given by

$$\begin{aligned}
&\psi_{k,1} = \frac{\sqrt{6}}{3}\phi_{k+1,1} - \frac{5\sqrt{3}}{9}\phi_{k+1,2} + \frac{2\sqrt{3}}{9}\phi_{k+1,3},\\
&\psi_{k,l} = \frac{1}{2}\phi_{k+1,2l-1} - \phi_{k+1,2l} + \frac{1}{2}\phi_{k+1,2l+1} && (k \ge 1,\ l = 2,3,\ldots,n_k-1),\\
&\psi_{k,n_k} = \frac{2\sqrt{3}}{9}\phi_{k+1,N_{k+1}-2} - \frac{5\sqrt{3}}{9}\phi_{k+1,N_{k+1}-1} + \frac{\sqrt{6}}{3}\phi_{k+1,N_{k+1}},
\end{aligned} \tag{71}$$

for $n=2$, and

$$\begin{aligned}
\psi_{k,1} &= 2\sqrt{\frac{3}{65}}\phi_{k+1,1} - \frac{77}{30}\sqrt{\frac{6}{65}}\phi_{k+1,2} + \frac{43}{15}\sqrt{\frac{6}{65}}\phi_{k+1,3} - \frac{17}{10}\sqrt{\frac{6}{65}}\phi_{k+1,4} + \frac{2}{5}\sqrt{\frac{6}{65}}\phi_{k+1,5},\\
\psi_{k,l} &= \frac{1}{\sqrt{42}}\phi_{k+1,2l-2} - 2\sqrt{\frac{2}{21}}\phi_{k+1,2l-1} + 3\sqrt{\frac{2}{21}}\phi_{k+1,2l}\\
&\qquad - 2\sqrt{\frac{2}{21}}\phi_{k+1,2l+1} + \frac{1}{\sqrt{42}}\phi_{k+1,2l+2} \qquad (l = 2,3,\ldots,n_k-1),\\
\psi_{k,n_k} &= \frac{2}{5}\sqrt{\frac{6}{65}}\phi_{k+1,N_{k+1}-4} - \frac{17}{10}\sqrt{\frac{6}{65}}\phi_{k+1,N_{k+1}-3} + \frac{43}{15}\sqrt{\frac{6}{65}}\phi_{k+1,N_{k+1}-2}\\
&\qquad - \frac{77}{30}\sqrt{\frac{6}{65}}\phi_{k+1,N_{k+1}-1} + 2\sqrt{\frac{3}{65}}\phi_{k+1,N_{k+1}},
\end{aligned} \tag{72}$$

for $n=4$. In equations (71) and (72), $n_k = 2^{k+1}(n=2)$ and $3\cdot 2^k(n=4)$, respectively.

5.4. Compression of coefficient matrices

Figure 10 depicts the memory requirement for the matrix entries. The piecewise constant wavelets mentioned above were used for the bases. In general, wavelet BEMs show highly

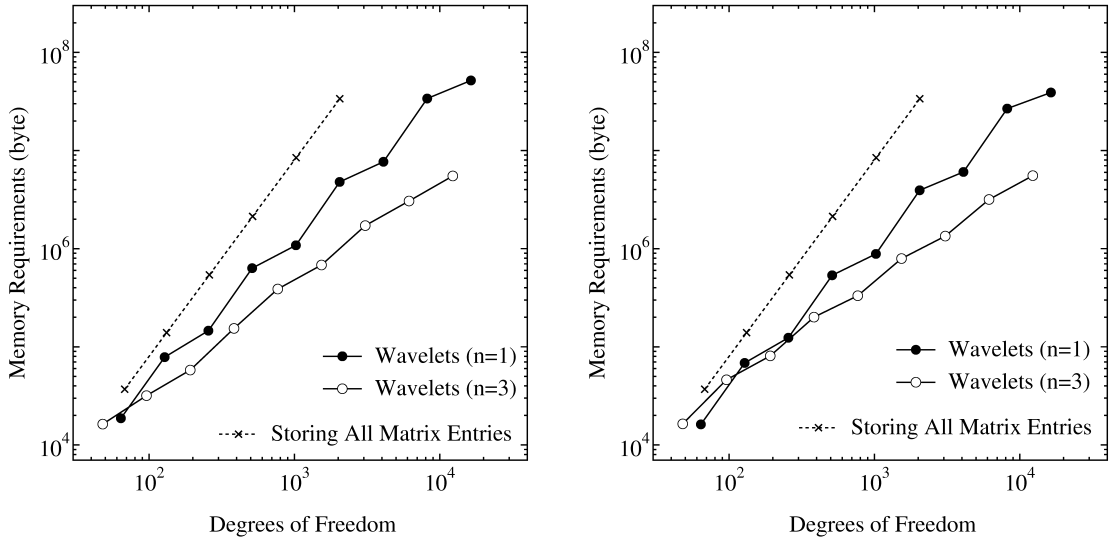

Figure 10: Memory requirements for matrix entries. Piecewise constant wavelets are used for the bases. (a) Ex.1. (b) Ex.2.

compression at a part of the coefficient matrix associated with fine-scale bases[7]. This effect can be enhanced by increasing the order of vanishing moments of wavelets[13]. The wavelets used in the previous studies, that is, orthonormal or semi-orthogonal wavelets, have a feature that the order of vanishing moments cannot be determined independently of the degree of polynomials. This obliges us to increase the degree of piecewise polynomials of wavelets, when we want to improve the sparseness of the matrices. On the other hand, the proposed wavelets allow us to enhance the compression of the matrix by only changing the order of vanishing moments. This fact is the obvious advantage of the present wavelets.

The rate of the stored matrix elements to all entries under the finest scale of the basis is summarized in Table 3. Note that the finest scale in the experiments was determined as $m_r = 11$ $(m = 0,\ n = 1)$, 9 $(m = 0,\ n = 3)$, 10 $(m = 1,\ n = 2)$ and 9 $(m = 1,\ n = 4)$. The matrices in the present examples are compressed to about 1% or less for the problems over 10000 DOF.

5.5. Reduction in CPU time

The CPU time for generating the matrix entries under each DOF in Ex.1 is shown in Figure 11. Throughout this paper, "conventional" in figures denotes the results corresponding to the usual boundary element equations in which *conventional* piecewise constant or linear functions and Galerkin method are used. The main advantage of the present wavelets is that one can choose the order of vanishing moments arbitrarily. While a highly compressed matrix can be obtained by increasing the order of vanishing moments, this fact sometimes leads to the disadvantage; the computational cost for generating the matrix

(a)

	Constant		Linear	
	$n=1$	$n=3$	$n=2$	$n=4$
DOFs	16384	12288	16388	12292
Rate of Compression (%)	1.61	0.30	1.60	0.50

(b)

	Constant		Linear	
	$n=1$	$n=3$	$n=2$	$n=4$
DOFs	16384	12288	16388	12292
Rate of Compression (%)	1.21	0.31	1.14	0.32

Table 3: Rate of the stored matrix elements to all entries under the finest scale. (a) Ex.1. (b) Ex.2.

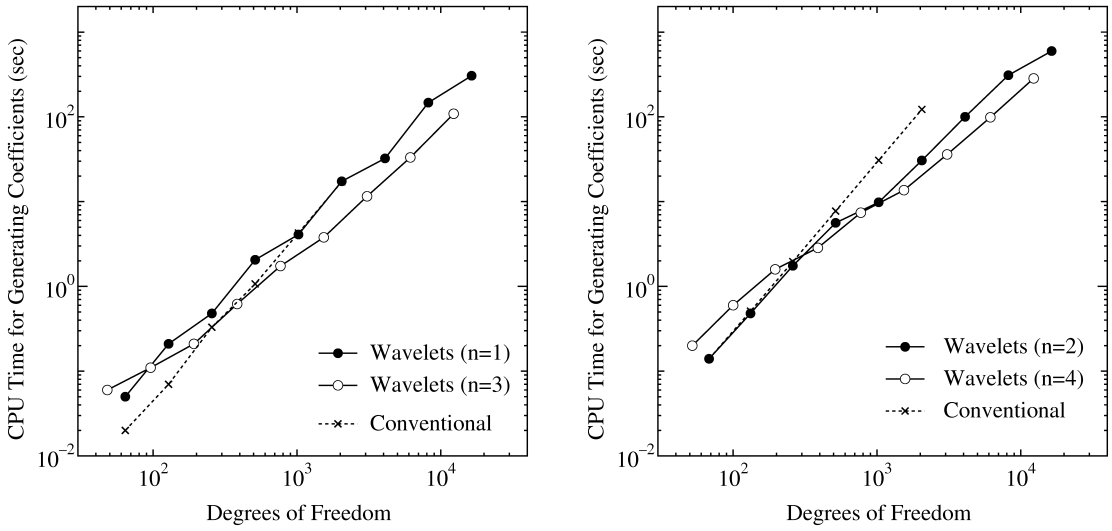

(a) (b)

Figure 11: CPU time for generating matrix entries in Ex.1. (a) Piecewise constant wavelets. (b) Piecewise linear wavelets.

entries raises considerably. This is because in the present wavelet the number of knots of splines increases with an increase in the order of vanishing moments. However, the numerical results show that the CPU time for computation of the matrix entries becomes shorter as the order of the vanishing moments increased, except for small DOFs. As a result, the matrix entries can be efficiently evaluated by truncating the small elements

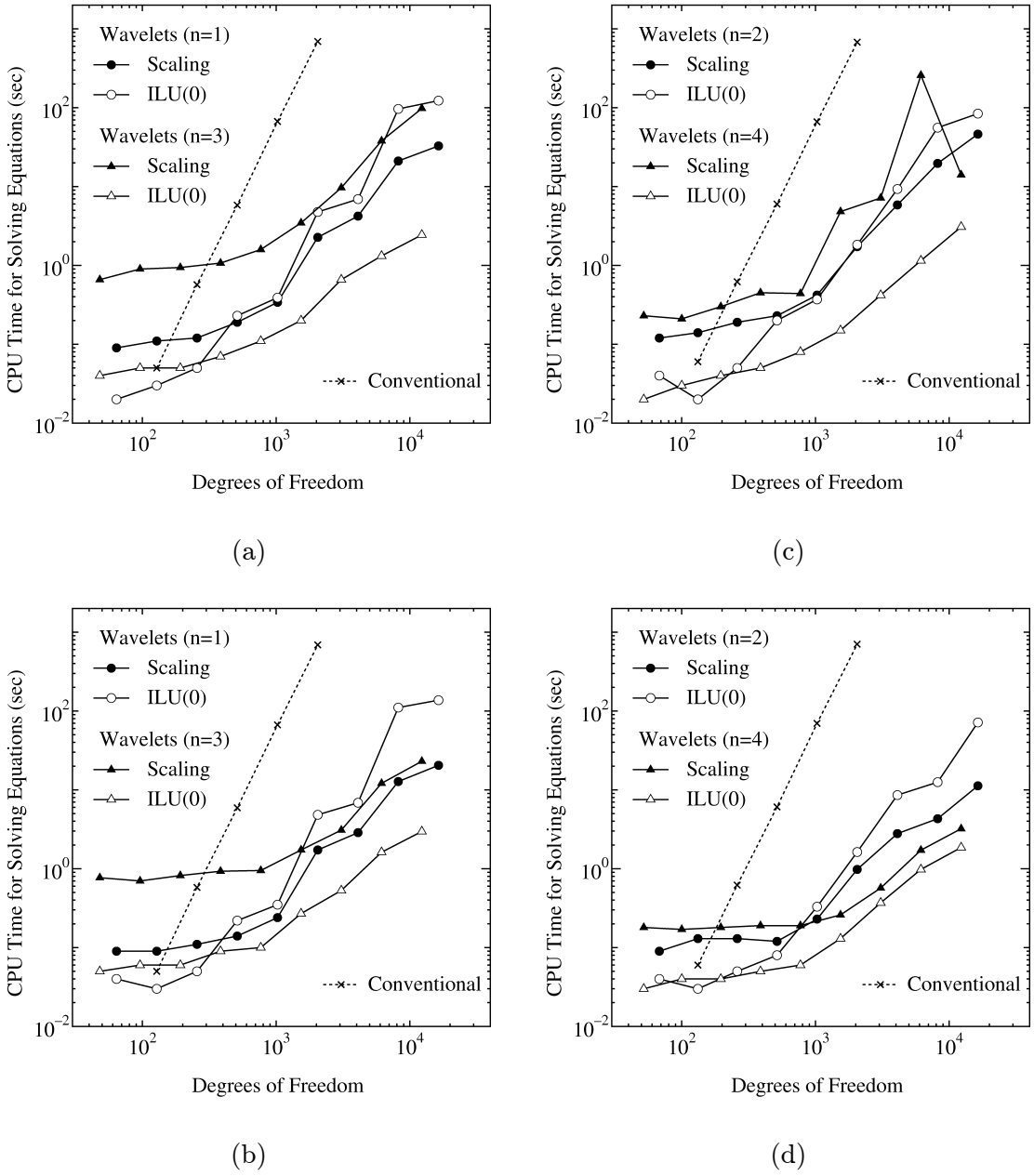

Figure 12: CPU time for solving the boundary element equations. (a) Piecewise constant wavelets (Ex.1). (b) Piecewise constant wavelets (Ex.2). (c) Piecewise linear wavelets (Ex.1). (d) Piecewise linear wavelets (Ex.2).

a priori. Moreover, it is advantageous for improvement of sparseness of the matrix to increase the order of vanishing moments.

Figure 12 shows CPU time for solving the boundary element equations. For small values of n, the convergence of iterative solution is rapid even if the diagonal scaling is employed as a preconditioner. Although the ILU(0) preconditioning improves convergence of the solution, it requires longer CPU time than the diagonal scaling because of lower

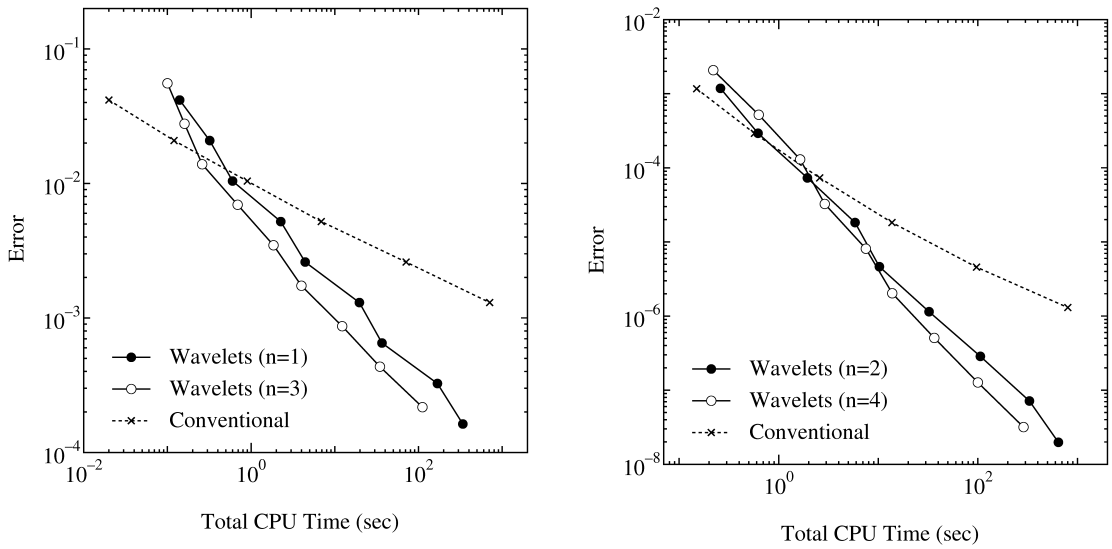

(a) (b)

Figure 13: Relation between total CPU time and L^2 norm of error in Ex.1. (a) Piecewise constant wavelets. (b) Piecewise linear wavelets.

sparseness of the matrix.

On the other hand, for the wavelets with greater n, the diagonal scaling is not necessarily useful preconditioning since a large number of iterations is required. As mentioned above, the computational work required at each iteration step becomes larger for the ILU(0) than for the diagonal scaling. However, it can be alleviated by increasing the sparseness of the matrix. Hence, for larger values of n, the ILU(0) becomes an effective preconditioner. Throughout these experiments, boundary element equations with the conventional bases were solved by Gauss elimination since the coefficient matrices are dense. In wavelet-BEM an iterative solver was employed to the equations with a sparse matrix. As a result, the CPU time is shortened comparing with the conventional method, particularly in large-scale problems.

Finally, the relation between the error and the total CPU time in Ex.1 is shown in Figure 13. Since the error seems to be independent of the order of vanishing moments under the optimal threshold parameter, it can be concluded that the total CPU time required to obtain solutions with certain accuracy can be reduced by increasing the order of vanishing moments.

6 Conclusions

We have presented construction of the compactly supported non-orthogonal B-spline wavelets with arbitrary order of vanishing moments. Efficiency of the proposed wavelets in boundary element analysis have been discussed. Unlike orthonormal or semi-orthogonal wavelets, any orthogonality is not required to these wavelets explicitly. However, this property does not lead to any disadvantages in BE analysis. Through numerical results, it

is found that we can save both memory requirement and CPU time by using the wavelets with higher order vanishing moments.

Since the wavelet-BEM deals with sparse matrices, an iterative solver is used to solve the boundary element equations. Therefore, we should choose a suitable preconditioner to obtain the solution rapidly. Efficiency of the preconditioner depends on sparseness of the coefficient matrix and convergence of iterative solution. Through numerical examples, it is suggested that the diagonal scaling becomes a suitable preconditioner for lower-order vanishing moments, while the ILU(0) becomes an effective for higher-order vanishing moments.

By increasing the order of vanishing moments, the number of knots of the spline wavelets are increased, and then the computational cost for construction of the coefficient matrix becomes expensive. Hence, it seems to be a drawback in the application of the wavelets with higher-order vanishing moments. However, truncating the small entries *a priori*, we can resolve this fear.

References

[1] Hackbusch W, Nowak ZP. On the fast matrix multiplication in the boundary element method by panel clustering. Numerische Mathematik 1989; 54: 463–491.

[2] Rokhlin V. Rapid solution of integral equations of classical potential theory. Journal of Computational Physics 1985; 60: 187–207.

[3] Beylkin G, Coifman R, Rokhlin V. Fast wavelet transforms and numerical algorithms I. Communications on Pure and Applied Mathematics 1991; 44: 141–183.

[4] Alpert B, Beylkin G, Coifman R, Rokhlin V. Wavelet-like bases for the fast solution of second-kind integral equations. SIAM Journal on Scientific Computing 1993; 14(1): 159–184.

[5] Canning FX. Sparse approximation for solving integral equations with oscillatory kernels. SIAM Journal on Scientific and Statistical Computing 1992; 13(1): 71–87.

[6] Rathsfeld A. A wavelet algorithm for the boundary element solution of a geodetic boundary value problem. Computer Methods in Applied Mechanics and Engineering 1998; 157: 267–287.

[7] Koro K, Abe K, Tazaki H. Application of discrete wavelet transform to wavelet collocation BEM. Journal of Applied Mechanics 1999; 2: 153–162. (in Japanese)

[8] Steinberg BZ, Leviatan Y. On the use of wavelet expansions in the method of moments. IEEE Transactions on Antennas and Propagation 1993; 41: 610–619.

[9] Sabetfakhri K, Katehi LBP. Analysis of integrated millimeter-wave and submillimeter-wave waveguides using orthonormal wavelet expansions. IEEE Transactions on Microwave Theory and Techniques 1994; 42(12): 2412–2422.

[10] Wang G. A hybrid wavelet expansion and boundary element analysis of electromagnetic scattering from conducting objects. IEEE Transactions on Antennas and Propagation 1995; 43(2): 170–178.

[11] Wang G. Application of wavelets on the interval to numerical analysis of integral equations in electromagnetic scattering problems. International Journal for Numerical Methods in Engineering 1997; 40: 1–13.

[12] Koro K, Abe K. H-hierarchical adaptive BEM with Haar wavelet functions for two-dimensional Laplace problems. In: Brebbia CA, Power H, editors, Boundary Element XXI, WIT Press, Southampton UK, 1999: 229–238.

[13] Goswami JC, Chen AK, Chui CK. On solving first-kind integral equations using wavelets on a bounded interval. IEEE Transactions on Antennas and Propagation 1995; 43(6): 614–622.

[14] Chui CK, Wang J. On compactly supported spline wavelets and a duality principle, Transactions of the American Mathematical Society 1992; 330 (2): 903–915.

[15] Williams JR, Amaratunga K. Introduction to wavelets in engineering. International Journal for Numerical Methods in Engineering 1994; 37: 2365–2388.

[16] Quak E, Weyrich N. Decomposition and reconstruction algorithms for spline wavelets on a bounded interval. Applied and Computational Harmonic Analysis 1994; 1: 217–231.

[17] Saad Y, Schultz MH. GMRES: A generalized minimal residual algorithm for solving nonsymmetric linear systems. SIAM Journal on Scientific and Statistical Computing 1986; 7 (3): 856–869.

[18] Petersdorff T, Schwab C. Wavelet approximations for first kind boundary integral equations on polygons. Numerische Mathematik 1996; 74: 479–519.

[19] Koro K, Abe K. Determination of optimal threshold for matrix compression in wavelet BEM. Boundary Elements XXIII, WIT Press, Southampton UK, 2001. (to appear)